Supporting Information

True- to sky-blue emitters bearing the thiazolo[5,4-*d*]thiazole electron acceptor for single and tandem organic light-emitting diodes

Abdelaziz Jouaiti,[a,] Dun-Cheng Huang,[b] Valerio Giuso,[c] Cristina Cebrián,[d] Pierluigi Mercandelli,[e] Kuan-Hsun Wang,[b] Chih-Hao Chang,[b,]* and Matteo Mauro[c,]**

[a] Laboratoire de Synthèse et Fonctions des Architectures Moléculaires, UMR7140 Chimie de la Matiere Complexe, Institut Le Bel, Université de Strasbourg & CNRS, 4 rue Blaise, Pascal 67000 Strasbourg (France), e-mail : jouaiti@unistra.fr

[b] Department of Electrical Engineering, Yuan Ze University, Chung-Li, 32003 Taiwan, e-mail: chc@saturn.yzu.edu.tw

[c] Institut de Physique et Chimie des Matériaux de Strasbourg (IPCMS) UMR7504, Université de Strasbourg & CNRS, 23 rue du Loess, 67083 Strasbourg (France), e-mail: mauro@unistra.fr

[d] Laboratoire Lorraine de Chimie Moléculaire (L2CM), Université de Lorraine, CNRS, F-57000 Metz, France

[e] Dipartimento di Chimica, Università degli Studi di Milano, via Camillo Golgi 19, 20133 Milano, Italy

Table of Contents

SUPPLEMENTARY METHODS

General consideration.

All reagents were used as received without further purification unless differently stated. Silica gel for column chromatography was purchased from Sigma-Aldrich. 4-(9*H*-carbazol-9-yl)benzaldehyde,[S1], 4-[3,6-bis(1,1-dimethylethyl)-9*H*-carbazol-9-yl]benzaldehyde[S2] and **TzTz-TPA2**,[S3] were prepared as described in the literature and their chemical characterization was in agreement with data reported previously. ^{1}H and ^{13}C NMR spectra were recorded at 298 K on either Bruker AV300, Bruker AV400 or Bruker AV500 spectrometers in deuterated solvents and the residual solvent peak was used as the internal reference. ^{1}H and ^{13}C{^{1}H} NMR spectra were calibrated to residual solvent signals. All the chemical shifts (δ) are reported in ppm. High-resolution electrospray mass spectrometry (HR-ESI-MS) was performed by the Service Spectrométrie de Masse of the Fédération de Chimie "Le Bel" FR2010 of the University of Strasbourg. Experimental details on synthesis are available in the Supporting Information.

Photophysical measurements

Instrument details. Steady-state emission spectra were recorded on a Horiba Jobin−Yvon IBH FL-322 Fluorolog 3 spectrometer equipped with a 450 W xenon arc lamp, double-grating excitation, and emission monochromators (2.1 nm mm^{-1} of dispersion; 1200 grooves mm^{-1}) and a Hamamatsu R13456 red sensitive Peltier-cooled PMT detector. Emission and excitation spectra were corrected for source intensity (lamp and grating) and emission spectral response (detector and grating) by standard correction curves. Time-resolved measurements were performed using either the Time-Correlated Single-Photon Counting (TCSPC) or the Multi-Channel Scaling (MCS) electronics option of the TimeHarp 260 board installed on a PicoQuant FluoTime 300 fluorimeter (PicoQuant GmbH, Germany), equipped with a PDL 820 laser pulse driver. A pulsed laser diode LDH-P-C-375 (λ = 375 nm, pulse full width at half maximum <50 ps, repetition rate 200 kHz–40 MHz) was

used to excite the sample and mounted directly on the sample chamber at 90°. The photons were collected by a PMA Hybrid-07 single photon counting detector. The data were acquired by using the commercially available software EasyTau II (PicoQuant GmbH, Germany), while data analysis was performed using the built-in software FluoFit (PicoQuant GmbH, Germany).

Alternatively, HORIBA-FluoroMax plus was used for fluorescence spectra and lifetime measurements. Time-resolved photoluminescence was measured by monitoring the intensity decay using the time-correlated single-photon counting technique with a nanosecond pulsed LED (λ_{ex} = 320 nm). All the PLQYs samples were recorded at a fixed excitation wavelength by using a Hamamatsu Photonics absolute PLQY measurements system Quantaurus QY equipped with CW Xenon light source (150 W), monochromator, integrating sphere, C7473 photonics multi-channel analyzer and employing the commercially available U6039-05 PLQY measurement software (Hamamatsu Photonics Ltd., Shizuoka, Japan). All measurements were repeated five times at the excitation wavelength λ_{exc} = 350–400 nm, unless otherwise stated.

Methods. For time resolved measurements, data fitting was performed by employing the maximum likelihood estimation (MLE) methods and the quality of the fit was assessed by inspection of the reduced χ^2 function and of the weighted residuals. For multi-exponential decays, the intensity, namely I*(t)*, has been assumed to decay as the sum of individual single exponential decays (Eqn. 1):

$$I(t) = \sum_{i=1}^{n} \alpha_i exp\left(-\frac{t}{\tau_i}\right) \qquad \text{eqn. 1}$$

where τ_i are the decay times and α_i are the amplitude of the component at t = 0. In the tables, the percentages to the pre-exponential factors, α_i, are listed upon normalization.

Computational details

Ground state and lowest-lying singlet excited state geometries were optimized by means of density functional and time-dependent density functional calculations. The parameter-free hybrid functional PBE0 [S4] was employed along with the standard valence double-ζ polarized basis set 6-31G(d,p) for C, H, N, O and S. All the calculations were done in the presence of solvent (dichloromethane, used in the photophysical characterizations) described by a polarizable continuum model (PCM) [S5]. The nature of all the stationary points was checked by computing vibrational frequencies and all the geometries were found to be true minima. A preliminary conformational analysis was performed, taking into account the rotation around all the bonds linking the rings and the rotation of the *tert*-butyl substituents on the *N*-carbazolyl groups. For all the three species the global minimum possesses an exact C_i point symmetry. In order to simulate the absorption electronic spectrum down to about 250 nm the lowest 30 singlet excitation energies were computed by means of time-dependent density functional calculations. The vibrationally-resolved emission spectra were simulated in the framework of the Franck-Condon principle [S6], shifting the 0–0 energy to its observed value. All the calculations were done with Gaussian 16 [S7].

OLED Devices Fabrication and Characterization

The used organic materials were purchased from Lumtec and Shine Materials Technology. All compounds were purified by temperature-gradient sublimation under a high vacuum before use. In sequence, the indium tin oxide (ITO) coated glass with a sheet resistance of ca. 15 Ω square^{-1} was washed with detergent solution, deionized water, and organic solvents. Then, the ITO glass was treated with a plasma jet for cleaning and enhancing the surface work function before the device was fabricated. The multiple organic layers and metal cathode were deposited on the ITO anode by vacuum evaporation in a vacuum chamber under the pressure of $<10^{-6}$ Torr and kept the deposition rates at around 0.1 nm s^{-1} and 0.5 nm s^{-1} for organic and metal structures, respectively.

The 2×2 mm active area of the device was defined by the shadow mask used for cathode deposition. Current-voltage-luminance (*J–V–L*) characterization used two Keithley 2401 equipped with a calibrated Si-photodiode as the current source and measurement to record data. The EL spectra of the devices were recorded using an Ocean Optics spectrometer.

References

(S1) Wang, X.-M.; Zhou, Y.-F.; Yu, W.-T.; Wang, C.; Fang, Q.; Jiang, M.-H.; Lei, H.; Wang, H.-Z. Two-Photon Pumped Lasing Stilbene-Type Chromophores Containing Various Terminal Donor Groups: Relationship between Lasing Efficiency and Intramolecular Charge Transfer. *J. Mater. Chem.* **2000**, *10*, 2698–2703. https://doi.org/10.1039/b006764o.

(S2) Fu, B.; Dong, X.; Yu, X.; Zhang, Z.; Sun, L.; Zhu, W.; Liang, X.; Xu, H. Meso-Borneol- and Meso-Carbazole-Substituted Porphyrins: Multifunctional Chromophores with Tunable Electronic Structures and Antitumor Activities. *New J. Chem.* **2021**, *45*, 2141–2146. https://doi.org/10.1039/d0nj02954h.

(S3) Ishi-i, T.; Ikeda, K.; Ogawa, M.; Kusakaki, Y. Light-Emitting Properties of Donor–Acceptor and Donor–Acceptor–Donor Dyes in Solution, Solid, and Aggregated States: Structure–Property Relationship of Emission Behavior. *RSC Adv.* **2015**, *5*, 89171–89187. https://doi.org/10.1039/c5ra18231j.

(S4) Called PBE1PBE in Gaussian. Adamo, C.; Barone, V. Toward Reliable Density Functional Methods without Adjustable Parameters: The PBE0 Model. *J. Chem. Phys.* **1999**, *110*, 6158–6170. https://doi.org/10.1063/1.478522.

(S5) Scalmani, G.; Frisch, M. J. Continuous Surface Charge Polarizable Continuum Models of Solvation. I. General Formalism. *J. Chem. Phys.* **2010**, *132*, 114110. https://doi.org/10.1063/1.3359469.

(S6) Barone, V.; Bloino, J.; Biczysko, M.; Santoro, F. Fully Integrated Approach to Compute Vibrationally Resolved Optical Spectra: From Small Molecules to Macrosystems. *J. Chem. Theory Comput.* **2009**, *5*, 540–554. https://doi.org/10.1021/ct8004744.

(S7) Gaussian 16 (revision A.03), Gaussian Inc., Wallingford, CT, 2016.

SUPPLEMENTARY FIGURES

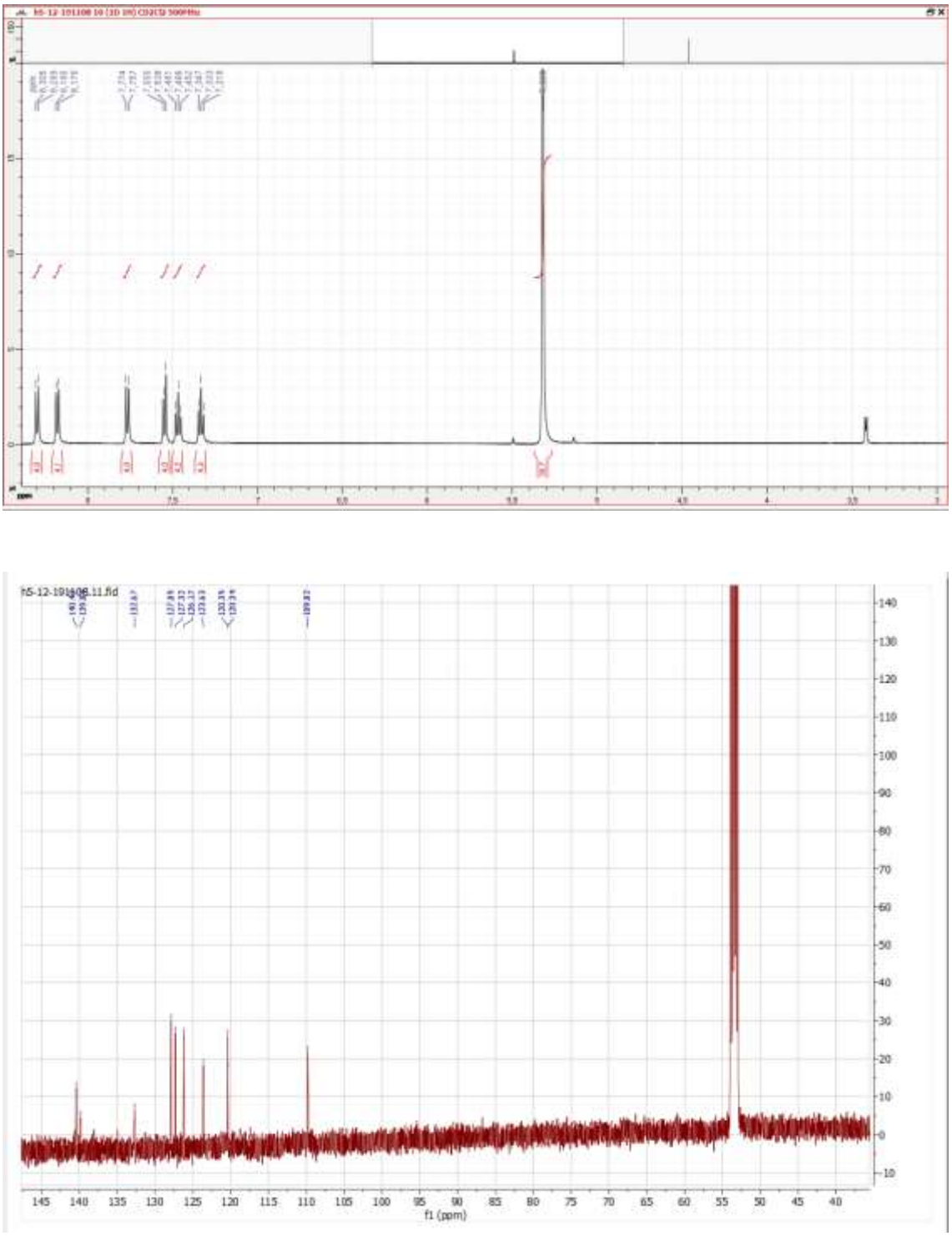

Figure S1. ^{1}H (500 MHz, *top*) and ^{13}C NMR (126 MHz, *bottom*) spectra recorded for compound **TzTz-PCz2** in $CDCl_3$ at 298 K.

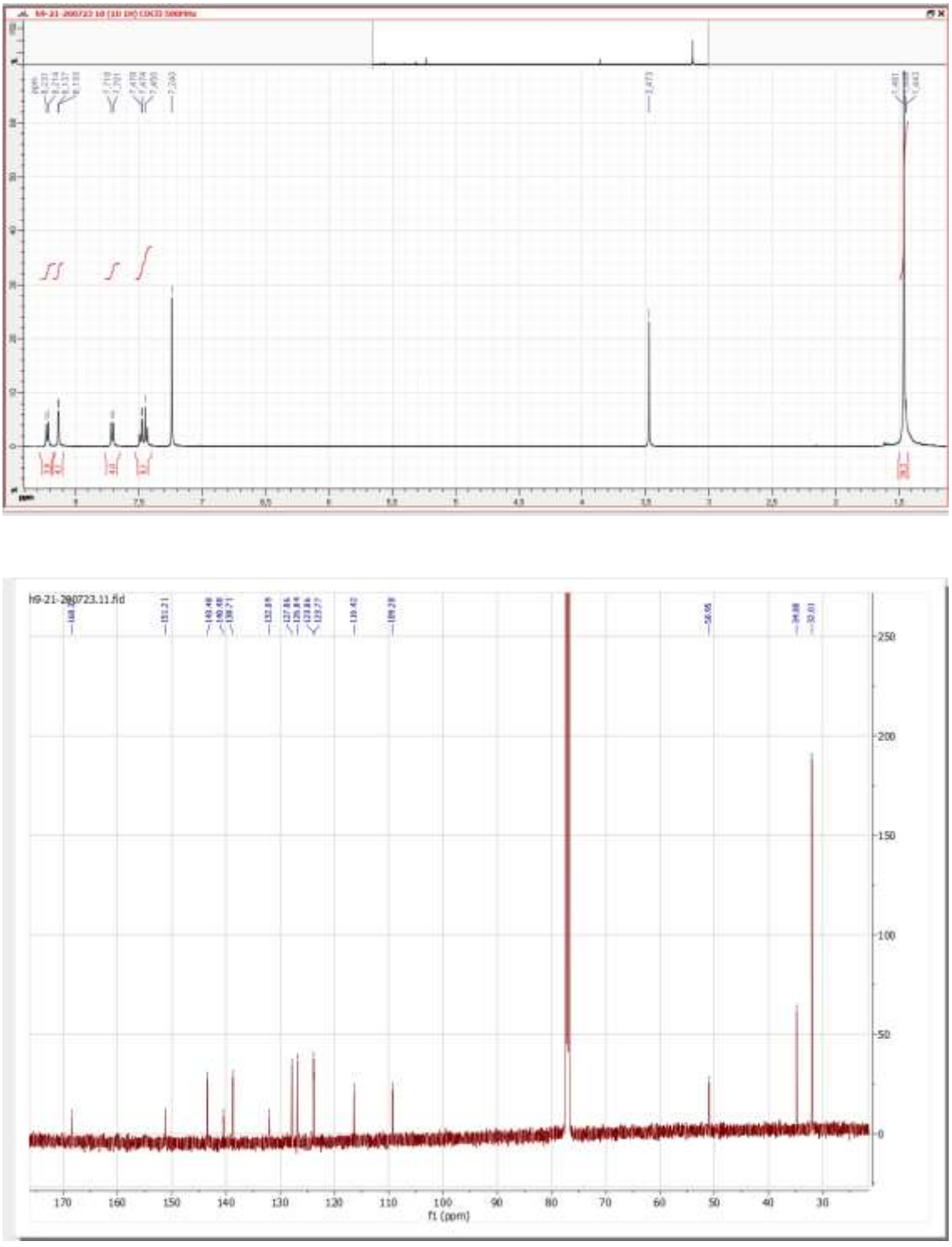

Figure S2. ^{1}H (500 MHz, *top*) and ^{13}C NMR (126 MHz, *bottom*) spectra recorded for compound **TzTz-PbtCz2** in $CDCl_3$ at 298 K.

Figure S3. High-resolution HR-ESI-MS spectrum of compound **TzTz-PCz2**.

Figure S4. High-resolution HR-ESI-MS spectrum of compound **TzTz-PbtCz2**.

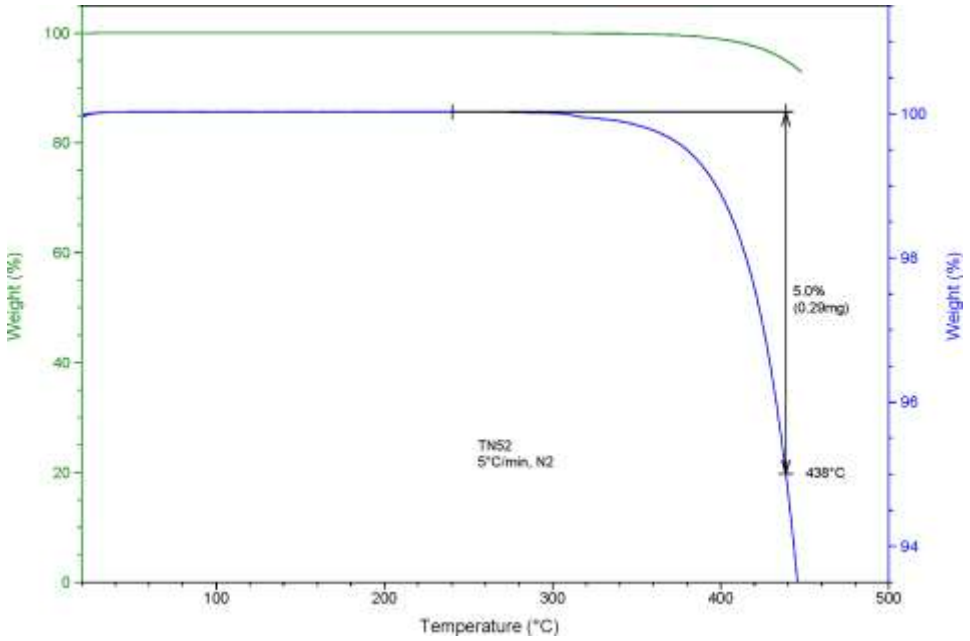

Figure S5. Thermogravimetric analysis recorded for compound **TzTz-PCz2**. Scan rate 5°C/min under N_2 atmosphere.

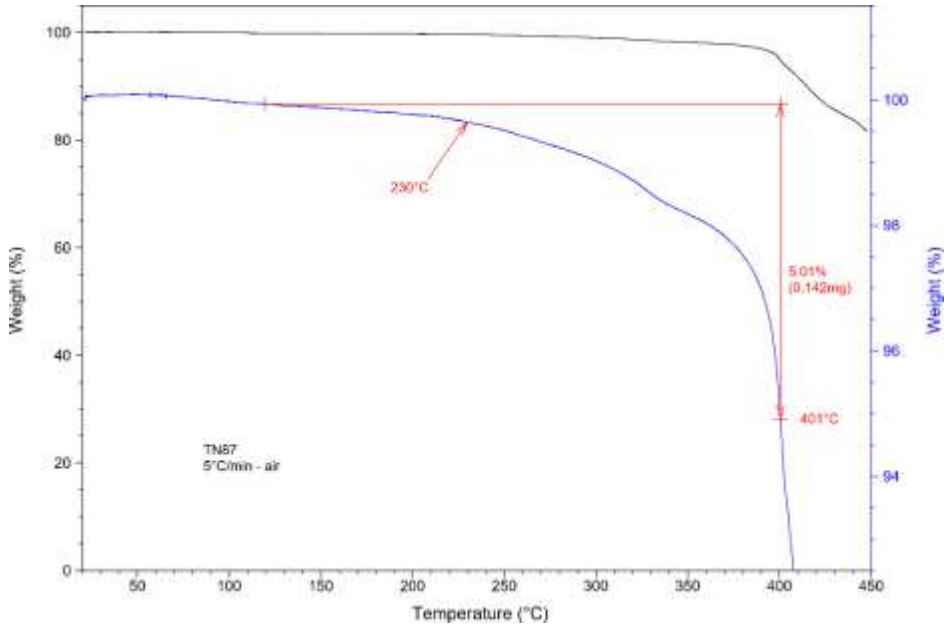

Figure S6. Thermogravimetric analysis recorded for compound **TzTz-PbtCz2**. Scan rate 5°C/min under N_2 atmosphere.

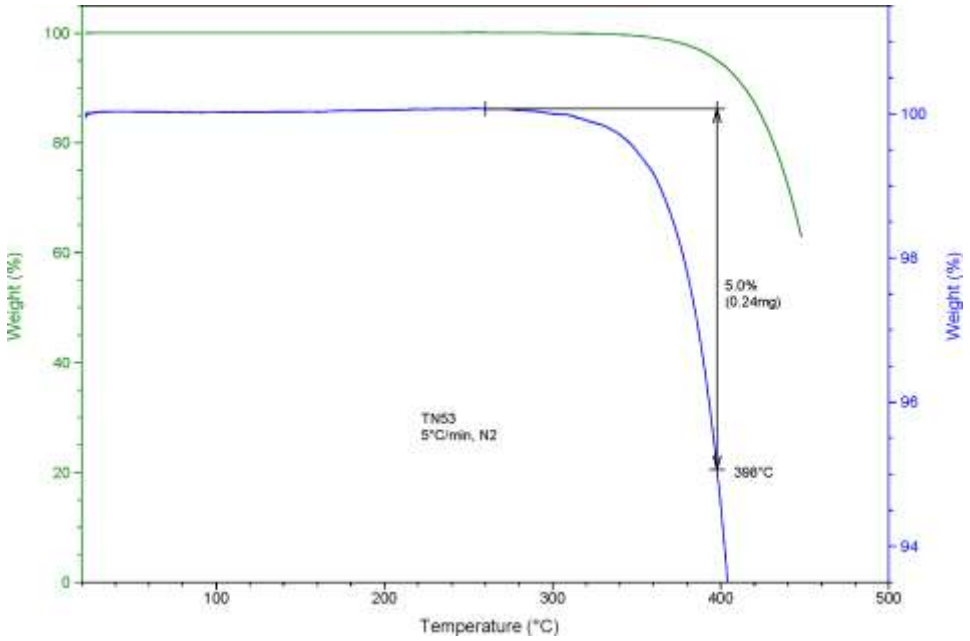

Figure S7. Thermogravimetric analysis recorded for compound **TzTz-TPA2**. Scan rate 5°C/min under N_2 atmosphere.

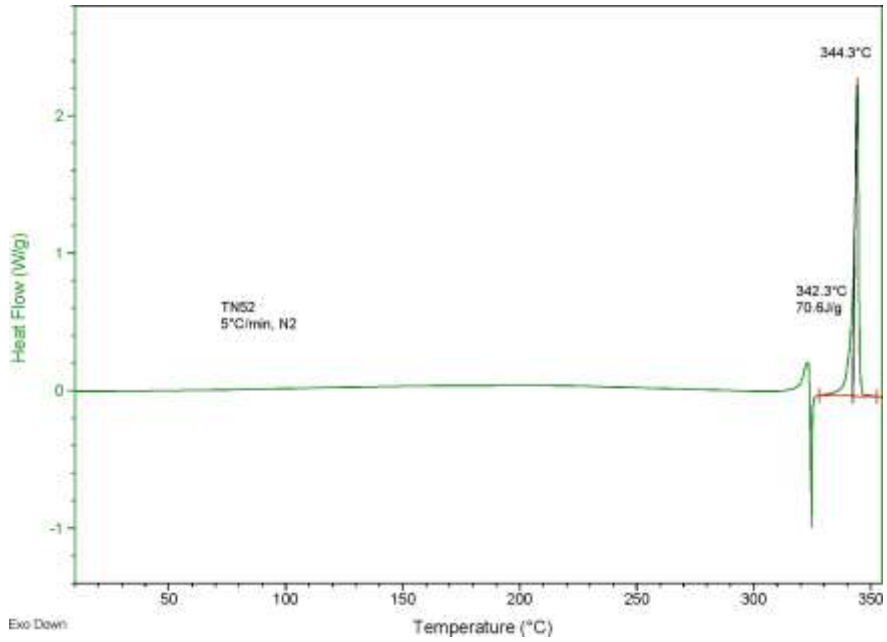

Figure S8. Differential scanning calorimetry (DSC) analysis recorded for compound **TzTz-PCz2**. Scan rate 5°C/min under N_2 atmosphere.

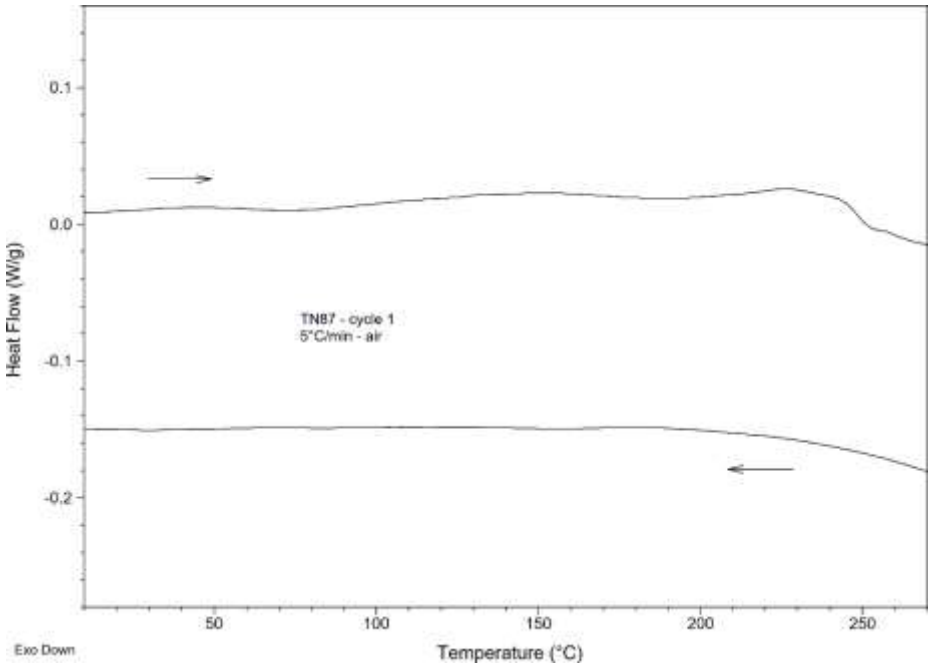

Figure S9. Differential scanning calorimetry (DSC) analysis recorded for compound **TzTz-PbtCz2**. Scan rate 5°C/min under N_2 atmosphere.

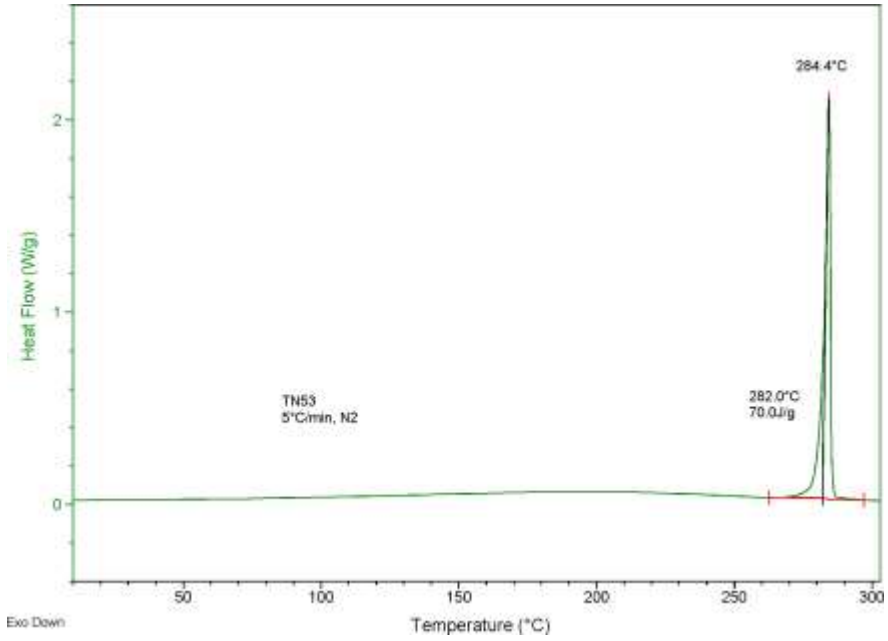

Figure S10. Differential scanning calorimetry (DSC) analysis recorded for compound **TzTz-TPA2**. Scan rate 5°C/min under N_2 atmosphere.

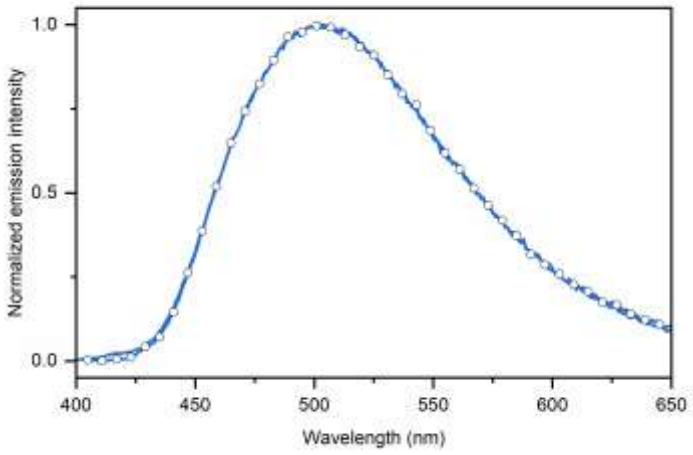

Figure S11. Comparison of the photoluminescence spectra recorded for compound **TzTz-PbtCz2** 3×10^{-6} M in acetone (blue trace) and acetone / TFA (1 M) (circles) at room temperature upon excitation at λ_{exc} = 380 nm.

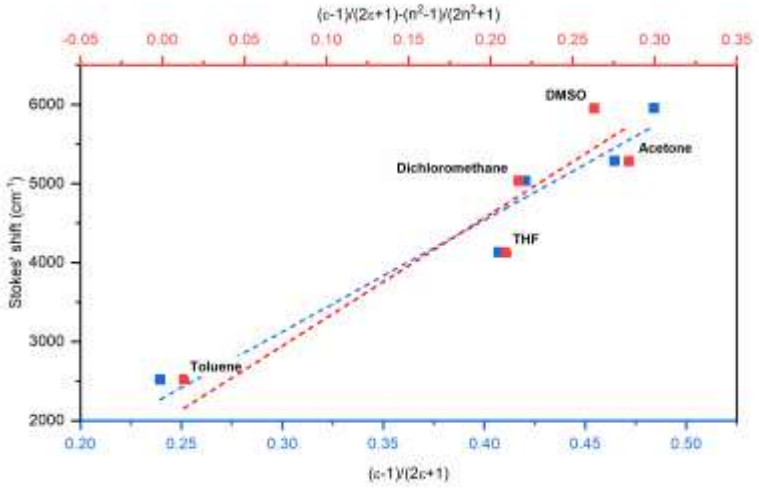

Equation	y = a + b*x
Plot	Stokes Shift
Intercept	-1119.03343 ± 31056.27625
Slope	14144.25329 ± 75411.60292

Equation	y = a + b*x
Plot	Stokes Shift
Intercept	1983.29867 ± 14190.03441
Slope	13170.10585 ± 65381.76694

Figure S12. Lippert-Mataga plot obtained for compound **TzTz-PbtCz2** in solvent of various polarities: plot of the observed Stokes shift (in wavenumber) as a function of solvent orientation polarizability, $\Delta f(\varepsilon_0, n)$ (red squares) and solvent permittivity (blue squares), using eqn. S1 and S2, respectively, defined as follows:

$$\bar{\nu}_{abs} - \bar{\nu}_{em} = \frac{2(\mu_e - \mu_g)^2}{hca^3}\left(\frac{\varepsilon_0 - 1}{2\varepsilon_0 + 1} - \frac{n^2 - 1}{2n^2 + 1}\right) + b'' \qquad \text{eqn. S1}$$

$$\bar{\nu}_{abs} - \bar{\nu}_{em} = \frac{2(\mu_e - \mu_g)^2}{hca^3}\left(\frac{\varepsilon_0 - 1}{2\varepsilon_0 + 1}\right) + b''' \qquad \text{eqn. S2}$$

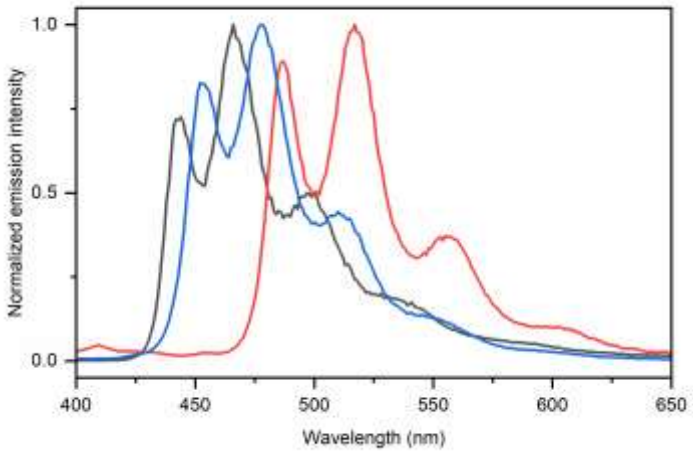

Figure S13. Photoluminescence spectra of compounds **TzTz-PCz2** (black), **TzTz-PbtCz2** (red) and **TzTz-TPA2** (blue) in 2-MeTHF glassy matrix at 77 K, upon excitation at λ_{exc} = 360 nm.

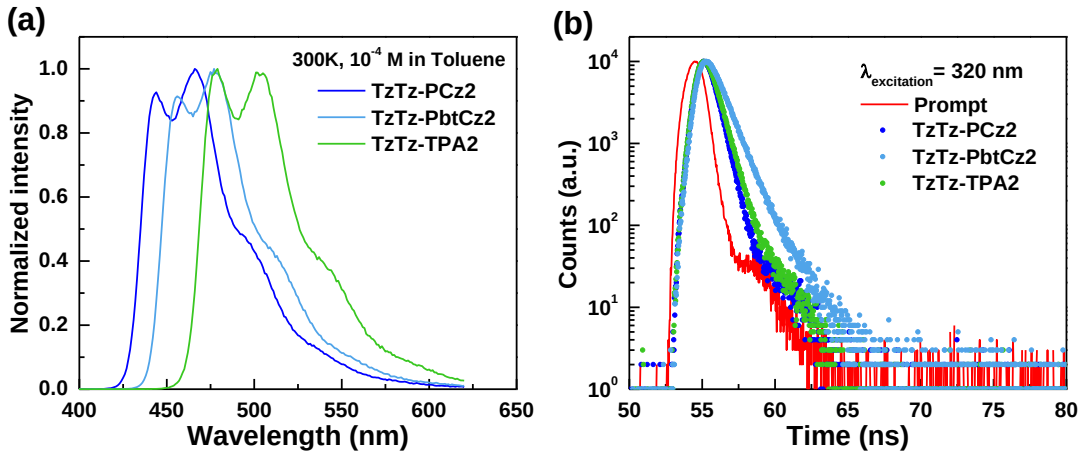

Figure S14. (a) PL spectra, and (b) decay characteristics of **TzTz-PCz2**, **TzTz-PbtCz2**, and **TzTz-TPA2**.

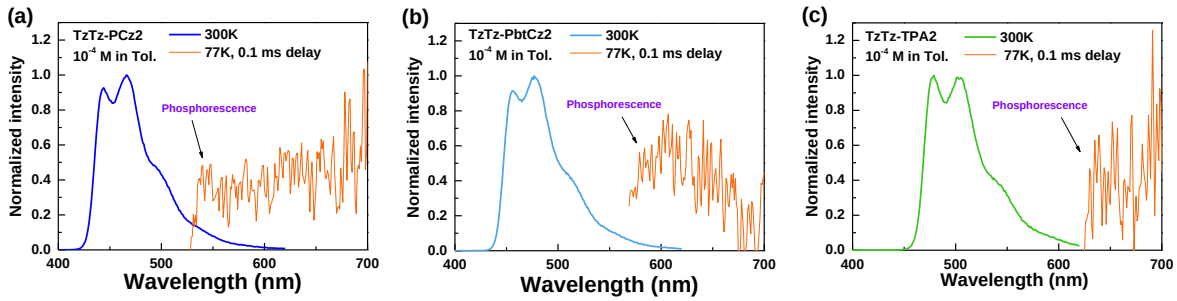

Figure S15. Fluorescent and phosphorescent spectra measured in toluene: (a) **TzTz-PCz2**; (b) **TzTz-PbtCz2**; (c) **TzTz-TPA2**.

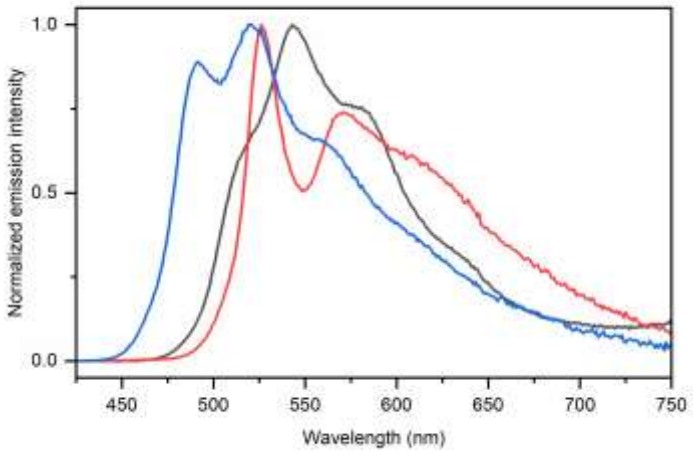

Figure S16. Photoluminescence spectra of solid-state samples as neat powder of compounds **TzTz-PCz2** (black), **TzTz-PbtCz2** (red) and **TzTz-TPA2** (blue) upon excitation at λ_{exc} = 400 nm.

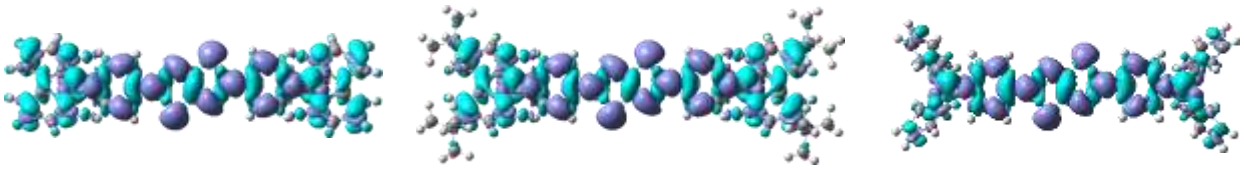

ΔE = 2.874 eV; λ = 431 nm	ΔE = 2.786 eV; λ = 445 nm	ΔE = 2.655 eV; λ = 467 nm
f = 1.5912	f = 1.6475	f = 2.0485
TzTz-PCz2	**TzTz-PbtCz2**	**TzTz-TPA2**

Figure S17. Electronic density-difference maps for the $S_0 \rightarrow S_1$ HOMO-LUMO excitation of **TzTz-PCz2**, **TzTz-PbtCz2**, and **TzTz-TPA2**. Cyan and violet indicates a decrease and increase in electron density, respectively.

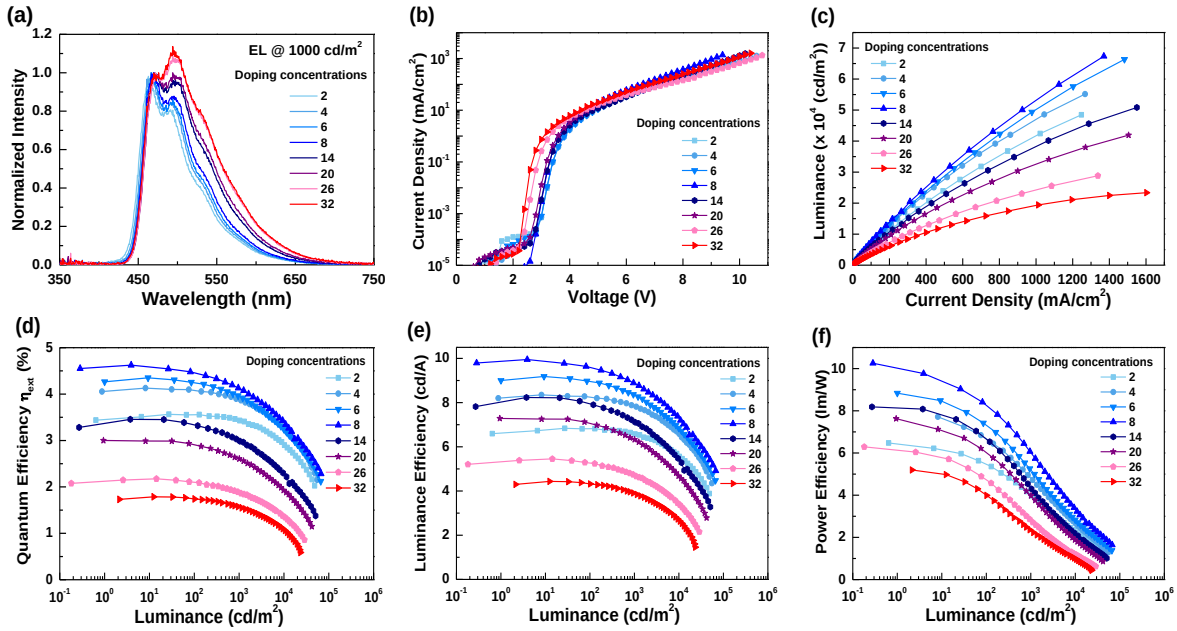

Figure S18. (a) Normalized EL spectra at a luminance of 10^3 cd m^{-2}; (b) current density−voltage (*J*−*V*) characteristics; (c) luminance−current density (*L*−*J*) characteristics; (d) external quantum efficiency vs luminance; (e) luminance efficiency vs luminance; (f) power efficiency vs luminance for **TzTz-PbtCz2**-based devices with different doping concentrations. [Device architecture: ITO (120 nm)/TAPC doped with MoO_3 10 wt.% (10 nm)/TAPC (20 nm)/TCTA (10 nm)/mCP doped with ***x*** wt.% **TzTz-PbtCz2** (30 nm)/TmPyPB (50 nm)/LiF (0.8 nm)/Al (120 nm), where ***x*** =2−32].

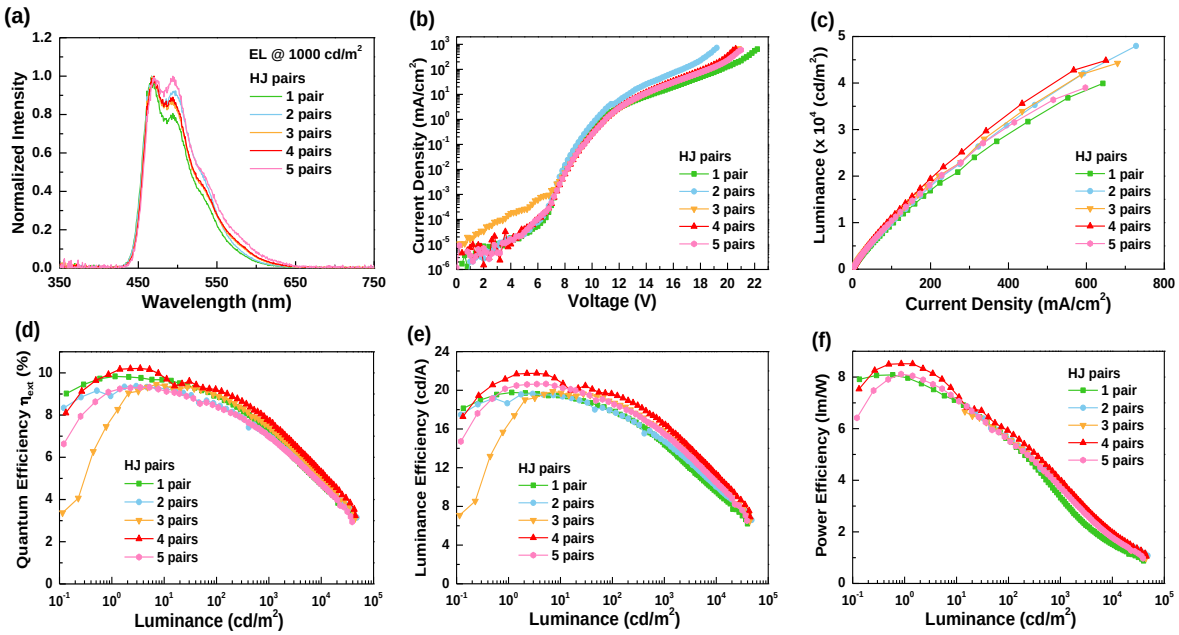

Figure S19. (a) Normalized EL spectra at a luminance of 10^3 cd m^{-2}; (b) current density−voltage (*J*−*V*) characteristics; (c) luminance−current density (*L*−*J*) characteristics; (d) external quantum efficiency vs luminance; (e) luminance efficiency vs luminance; (f) power efficiency vs luminance for tandem device BT with different OHJ pairs.

SUPPLEMENTARY TABLE

Table S1. EL characteristics of tandem device BT with different HJ pairs.

Device		BT (TzTz-PbtCz2)				
HJ pairs in CGL		**1**	**2**	**3**	**4**	**5**
External Quantum Efficiency (%)	[a]	9.8	9.4	9.5	10.2	9.3
	[b]	8.9	8.5	8.9	9.2	8.4
Luminance Efficiency (cd A^{-1})	[a]	19.8	19.6	19.9	21.8	20.7
	[b]	17.9	17.8	18.8	19.6	18.6
Power Efficiency (lm W^{-1})	[a]	8.1	8.1	7.3	8.5	8.1
	[b]	5.6	6.7	5.6	5.9	5.6
V_{on} (V)	[c]	7.7	7.6	7.9	7.9	7.9
λ_{peak} (nm)	[d]	467	467	470	470	470
Max Luminance (cd m^{-2}) [V]		39916 [22.2]	47972 [19.2]	44275 [20.8]	44851 [20.6]	39004 [21.0]
CIE1931 coordinates (x, y)	[b]	(0.16, 0.31)	(0.16, 0.34)	(0.17, 0.33)	(0.18, 0.32)	(0.18, 0.36)
	[d]	(0.16, 0.30)	(0.16, 0.33)	(0.17, 0.33)	(0.17, 0.31)	(0.18, 0.36)

[a] Maximum efficiency; [b] measured at 10^2 cd m^{-2}; [c] turn-on voltage measured at 1 cd m^{-2}; measured at 10^3 cd m^{-2}.